

# SENSING THE EARTH'S LOW IONOSPHERE DURING SOLAR FLARES USING VLF SIGNALS AND GOES SOLAR X-RAY DATA

Aleksandra Kolarski<sup>a,\*</sup>, Davorka Grubor<sup>b</sup>

<sup>a</sup>*Institute for Geophysics, Batajnički drum 8, 11000 Belgrade, Serbia*

<sup>b</sup>*Faculty of Mining and Geology, Physics Cathedra, University of Belgrade, Džušina 7,  
11000 Belgrade, Serbia*

---

## Abstract

An analysis of D-region electron density height profile variations, induced by four isolated solar X-ray flares during period from September 2005 to December 2006, based on the amplitude and the phase delay perturbation of 22.1 kHz signal trace from Skelton (54.72 N, 2.88 W) to Belgrade (44.85 N, 20.38 E), coded GQD, was carried out. Solar flare data were taken from NOAA GOES12 satellite one-minute listings. For VLF data acquisition and recordings at the Institute of Physics, Belgrade, Serbia, the AbsPAL system was used. Starting from LWPCv21 code ([Ferguson, 1998](#)), the variations of the Earth-ionosphere waveguide characteristic parameters, sharpness and reflection height, were estimated during the flare conditions. It was found that solar flare events affected the VLF wave propagation in the Earth-ionosphere waveguide by changing the lower ionosphere electron density height profile, in a different way, for different solar flare events.

*Keywords:* solar X-ray flare, VLF wave, Earth-ionosphere waveguide

---



---

\*Corresponding author

*Email addresses:* [aleksandrakolarski@gmail.com](mailto:aleksandrakolarski@gmail.com) (Aleksandra Kolarski),  
[davorkag@eunet.rs](mailto:davorkag@eunet.rs) (Davorka Grubor)

## 1. Introduction

Production of electrons in D-region (which extends in altitude between a range of heights from 50 km to 90 km) in unperturbed ionospheric conditions is mainly related to the photoionization processes, UV Lyman- $\alpha$  spectral line 121.6 nm, EUV spectral lines ranging from 102.7 nm to 118.8 nm and galactic cosmic rays. Different space phenomena, like X-ray solar flares (Thomson et al., 2005), solar eclipse (Chakrabarti et al., 2012b), CME (Balan et al., 2008),  $\gamma$ -ray bursts (Inan et al., 2007; Chakrabarti et al., 2010), solar terminator (Nina and Čadež, 2013a), affect the changes in intensity of the incidence of radiation in D-region and consequently change the electron density time and space distributions.

During the flare events, the ionization in the lower ionosphere, induced by electromagnetic radiation from the solar X-ray range (0.1-0.8 nm), significantly exceeds the ionization of all the regular ionization factors (such as Lyman- $\alpha$  spectral line 121.6 nm and cosmic rays) and causes photoionization of neutral constituents in the lower ionosphere, becoming a major source of ionization in this region (Whitten and Poppoff, 1965). Electron density increases as a result of additional ionization of the lower ionosphere constituents and thus changes the lower ionosphere electron density height profile, affecting the Earth-ionosphere waveguide characteristics (Mitra, 1974).

Electron density in the ionosphere can be determined according to many different methods, including the rocket probes, radar measurements and the technique using radio wave signals (Belenkiy et al., 2006; McKinnell and Friedrich, 2007; Žigman et al., 2007; Chakrabarti et al., 2012a). As in many other manuscripts (Pal and Chakrabarti, 2010; Basak and Chakrabarti, 2013; Nina et al., 2012b; Thomson et al., 2011), for monitoring of the lower ionosphere, Very Low Frequency (VLF) radio signals are used in this paper as well. One of the widely used procedures for electron density calculations from VLF data is based on the application of Wait theory and LWPC (Long Wave Propagation Capability (Ferguson, 1998)) numeric routine code (McRae and Thomson, 2000; Grubor et al., 2008; Žigman et al., 2007; Thomson et al., 2011; Kolarski et al., 2011; Nina et al., 2011, 2012a,b).

Propagating VLF signal amplitude and phase delay, otherwise stable under undisturbed solar conditions (Thomson, 1993; McRae and Thomson, 2000), undergo perturbations since the VLF signal propagation parameters change as a consequence of electron density increase in the lower ionosphere induced by the solar X-ray flare events. Electron production rate coefficient

can be considered as directly proportional to ionizing X-ray radiation intensity (Ratcliffe, 1972; Budden, 1988) (a typical representation of electron density responses to the incidence of X-ray radiation at different altitudes is given in (Nina et al., 2012b)) and that is the reason why it is possible to draw conclusions about the simultaneous changes of electron density height profiles in D-region by analyzing VLF signals recorded during the solar flare events, as it is shown in this paper.

The Absolute Phase and Amplitude Logger (AbsPAL) receiving system, located at Institute of Physics in Belgrade, was used for receiving, monitoring and for the storage of amplitude and phase delay of VLF data on frequency 22.1 kHz (GQD signal emitted from Skelton, UK). The phase delay and amplitude signal perturbations on GQD/22.1 kHz signal traces, produced by C and M class isolated X-ray solar flare events at equinox, winter and summer season, were studied and are presented in this paper.

## 2. Results and Discussion

The GQD signal propagates WNW-ESE along a short Great Circle Path ( $D_{GCP} = 1980$  km) and mostly an overland path (Figure 1). The X-ray (0.1-0.8 nm) flare events, according to NOAA GOES12 one-minute data listings, used in the following exemplary analysis are given in Table 1.

The VLF signal perturbations related to analyzed solar flare events, observed on GQD/22.1 kHz signal traces, in periods enclosing the flare events on the perturbed days, are shown in Figures 2-5 using the solid lines (phase delay on upper plots and amplitude on lower plots), respectively. The diurnal phase delay and amplitude variations for GQD/22.1 kHz signal traces, in the same daytime periods, but on the quiet days considered, are added to the upper and lower panels of Figures 2-5 and are presented with the dotted lines. The X-ray irradiances during the periods of the flare events impact are added to the upper panels of Figures 2-5 (outer right axes) and are presented using the dashed lines. Characteristic signal states during the analyzed flare events are marked by arrows.

As evident from Figures 2-5, solar X-ray flares caused phase delay and amplitude perturbations on GQD signal traces. However, the "pattern" of perturbations is not the same for these events. The reason for such a behavior is that analyzed signals are propagating through the different waveguides due to diurnal and seasonal changes of the lower ionosphere and because of the different events' characteristics. The common feature for all four events is

peak amplitude time delay,  $\Delta t = 1 - 2$  min, after the peak of X-ray irradiance, and it was attributed to the "sluggishness" of the ionosphere in reaching the peak electron density in D-region, induced by flare and caused by recombination processes (Mitra, 1974; Appleton, 1953; Žigman et al., 2007; Nina et al., 2012b). The amplitude and phase delay GQD signal perturbations during analyzed flare events have oscillatory character, and the type of oscillations is related to the class of the observed solar flare event (Grubor et al., 2008).

The incidence of the X-ray radiation in the Earth's ionosphere during the solar flare causes not only an enhancement of the maximum electron density, but it also changes the distribution of ionization from an upper to a lower edge of the D-region. The propagation model (Wait and Spies, 1964) considered the electron density  $N_e$  ( $\text{m}^{-3}$ ) in the waveguide at the altitude  $z$  (km), by two parameters: reflecting edge sharpness, denoted by  $\beta$  ( $\text{km}^{-1}$ ) and reflecting edge height, denoted by  $H'$  (km):

$$N_e(z, H', \beta) = 1.43 \cdot 10^{13} e^{-0.15H'} e^{(\beta-0.15)(z-H')} . \quad (1)$$

This model has been used to simulate VLF propagation through the Earth-ionosphere waveguide at regular conditions (Thomson, 1993; McRae and Thomson, 2000), as well as for the conditions corresponding to the flare peak irradiance (McRae and Thomson, 2004; Thomson et al., 2005). The Earth-ionosphere waveguide was modeled for several characteristic moments during each flare event and the results obtained are in line with VLF signal measurements.

By means of a LWPCv21 code, the propagation paths of VLF wave on frequency 22.1 kHz were simulated with a goal to estimate the best fitting pairs of parameters ( $\beta$ ,  $H'$ ) to yield values closest to a real measured phase delay and the amplitude at the Belgrade receiver site, for each characteristic state of each considered flare event.

LWPC is a set of several separate programs, each designed for implementation of specific operations. LWPM program (Long Wave Propagation Model) implies a standard model of the ionosphere with an exponential conductivity increase with height. LWPC program takes values  $\beta = 0.30 \text{ km}^{-1}$  and  $H' = 74 \text{ km}$ , as standard values for regular (unperturbed) daytime ionosphere conditions. In order to simulate propagation conditions held in the perturbed waveguide during the flare impact, it is necessary to modify a propagation model, using LWPC subprogram REXP (Range Exponential Model) which calculates the phase delay and the amplitude of the given VLF signal, de-

pending on a chosen GCP path and corresponding pairs of  $(\beta, H')$  parameters as impute parameters defined by the user. If pairs of  $(\beta, H')$  parameters are correctly defined, then the numerically simulated VLF signal phase delay and amplitude values will be very close to the measured values of VLF signal for a given signal trace.

Since parameters  $(\beta, H')$  change along the signal trace, in case of a GQD signal which propagates along the path 1980 km long from a transmitter to a receiver, it corresponds to one time zone. For this purpose, the constant "average value" of otherwise variable parameters  $\beta, H'$  was chosen and used along the whole trace for the analyzed signals, depicting "average ionospheric conditions" held along the whole trace for each simulation.

Perturbed phase delay and amplitude values, at characteristic states during the flare impact, were denoted as  $P_{flare}$  and  $A_{flare}$ , depending on each particular case, while corresponding phase delay and amplitude regular values at quiet days were denoted as  $P_{reg}$  and  $A_{reg}$ . For getting perturbed values of simulated phase delay and amplitude,  $P_{flare}$  and  $A_{flare}$ , for all flare events, perturbed values of  $(\beta, H')$  pairs of parameters defined using REXP routine, were used. For this purpose, the procedure of succeeding probe iterations was used. Depending on type of perturbation, phase delay and amplitude perturbations,  $\Delta P$  ( $^{\circ}$ ) and  $\Delta A$  (dB), can be positive or negative values, and were calculated as:  $\Delta P = P_{flare} - P_{reg}$ , and  $\Delta A = A_{flare} - A_{reg}$ .

The calculated amplitude and phase delay values obtained by LWPCv21 code are in good agreement with the measured values at the Belgrade receiver site. Therefore, it can be further assumed that numerically modeled signals had been transmitted in modeled ionospheric conditions which are in good agreement with real ionospheric conditions held at the time and measured at the place of the receiver site. The measured phase delay and amplitude perturbations and estimated corresponding parameters  $(\beta, H')$  and corresponding electron densities at 74 km, calculated using (1) at three characteristic moments that correspond to the unperturbed (preflare) state, perturbed flare state and the "recovered" postflare state during the analyzed flare events, are given in Table 2.

The errors introduced by the technique used have been critically examined to place the uncertainty of the results arrived at between 10% and 20%. Also, deviations in determining electron concentrations using different models vary for different altitudes. According to the analysis for perturbed flare state ( $I_{xmax}$ ) given in (Grubor et al., 2008), electron density ratios are within one order of magnitude, while in case of unperturbed flare state given

in (Nina and Čadež, 2013b) electron density ratios are smaller. There are numerous techniques, some more precise, for determining ionospheric parameters and electron densities that include complicated ionospheric chemistry and sophisticated numerical codes (Basak and Chakrabarti, 2013; Nina et al., 2012b; Žigman et al., 2007; Palit et al., 2013; Tanaka, 2010), but taking into account that errors related to determining of ionospheric parameters by using different methods are about one order of magnitude (factor 10), for the purpose of qualitative analysis conducted in this work, results obtained by applied Wait theory and LWPC numeric code are quite satisfactory.

For all characteristic times (marked with arrows in Figures 2-5) during the analyzed flare events, the vertical electron density height profiles through ionospheric D-region (50 - 90 km altitude range) were calculated using (1). Corresponding  $N_e$  at altitude 74 km for all analyzed characteristic times are given in Table 2. Since the GQD signal amplitude and phase delay perturbations especially in case of C9.7 and M2.5 X-ray flare events (07 April, 2006 and 06 July, 2006, respectively), are quite complex, for a clearer view only changes of the electron density height profiles related to unperturbed pre-flare state (dotted lines), perturbed flare state (solid lines) and "recovered" postflare state (dashed lines) of ionospheric conditions for each flare event are shown in Figures 6-9. The changes of electron density height profiles for GQD signal traces at ionospheric D-region bottom (50 km) and at ionospheric D-region top (90 km) should be taken with caution, because of the possible failure of the model at the D-region boundaries. Nevertheless, the changes of electron density height profiles at 74 km altitude are realistic, and  $N_e(74 \text{ km})$  for the flare events considered is in line with results of other studies (Žigman et al., 2007; McRae and Thomson, 2004; Kolarski et al., 2011; Nina et al., 2011, 2012a).

Amplitude and phase delay VLF signal values computed by means of LWPC code, which have been chosen as the best fitting to the real measured amplitude and phase delay at the receiver site, are the last values in the series of values that the program code computes for every point on the signal path, based on the corresponding propagation model of the wave package inside the waveguide. If the chosen pair of  $(\beta, H')$  parameters reproduces the values of a measured amplitude and phase delay at the receiver site well, then all the computed values of amplitude and the phase delay for every point on the signal path can be considered reliable. In other words, for every moment of the change in the waveguide state conditions, the signal amplitude and phase delay changes depending on the location along the GCP, can be simulated.

One should bear in mind that the chosen pair of  $(\beta, H')$  parameters depicts "average ionospheric conditions" in the waveguide and in case of GQD signal trace, the GCP distance is 1980 km and it covers fewer than two time zones.

The GQD signal amplitude and phase delay changes along the GCP, caused by the four X-ray solar flare events considered, were analyzed for preflare, flare and postflare states. The changes of the amplitude and phase delay at the site of the main modal minimum and at the site of the receiver were analyzed and also the morphology and the changes of the location of the main modal minimum during considered solar flare events. For GQD signal trace analyzed in this paper, the most prominent changes in the waveguide state, caused by the incidence of X-ray radiation during the solar flare events, occur at the location of the main modal minimum and not at the receiver site. During all the solar flare events considered (especially in case of C9.7, M2.5 and C9.6 flare events), the main modal minimum of GQD signal becomes mitigated and moves toward the transmitter, although in case of the weak C4.8 flare event changes of the main modal minimum characteristics and location are negligible.

Simulation results of GQD signal amplitude and phase delay changes along the GCP are given in Table 3, where symbol  $\uparrow$  denotes the main modal minimum mitigation in the flare state,  $r$  is the ratio between the simulated GQD signal amplitude at the main modal minimum in postflare and preflare state:  $r = A_{simpostflare}/A_{simpreflare}$ ,  $D$  (km) is the distance between the main modal minimum and the transmitter in preflare ( $D_{preflare}$ ), flare ( $D_{flare}$ ) and postflare ( $D_{postflare}$ ) state,  $\Delta D$  (km) is the difference in the main modal minimum location between postflare and preflare state:  $\Delta D = D_{postflare} - D_{preflare}$  and  $\Delta D_f$  (km) is the difference in the main modal minimum location between the flare and preflare state:  $\Delta D_f = D_{flare} - D_{preflare}$ .

In the flare state in case of C9.7 flare event, the amplitude and phase delay minimum tended to form at the receiver site (denoted with "\*\*" in Table 3) which additionally lowered the registered amplitude and phase delay. In the flare state in case of M2.5 flare event, at 1760 km away from the transmitter, an additional modal minimum was formed, which led to a slight increase in the amplitude and a decrease in the phase delay registered at the receiver site. In the flare state in case of C9.6 flare event, at 1760 km away from the transmitter, an additional modal minimum was formed, which led to an increase in the amplitude followed by a decrease in the phase delay registered at the receiver site. Flare event of C4.8 class did not significantly change the waveguide characteristics and it relatively weakly affected GQD signal



amplitude and the phase delay variation along the GCP.

After the impact of C9.7 and C9.6 solar flare events, the propagation conditions in the GQD signal waveguide returned to the regular and established signal amplitude and phase delay variation along the GCP in postflare state was almost identical as in the preflare state (parameters  $r$  and  $\Delta D$  in Table 3). In the state of recovered ionospheric conditions after the C4.8 solar flare event impact, a secondary modal minimum at 760 km away from the transmitter became more pronounced than the modal minimum considered as the main in preflare and post flare states (denoted with "\*" in Table 3). It should be noted that the recovery for this flare event lasted for 41 minutes and also that the ionosphere before this flare event occurred had already been perturbed by a strong flare event of M6 class which occurred earlier that day at 08:22UT, so that the ionosphere actually got back to its regular state after the C4.8 solar flare event, at 12:59UT. Only M2.5 flare event, also the strongest of the flare events considered, had left more lasting effects on the GQD signal waveguide.

Deviations from the characteristic VLF signal amplitude and phase delay variation scheme indicate that the disturbance in the Earth-ionosphere waveguide took place. Such changes of the waveguide characteristics can cause different types of changes in the amplitude and phase delay, with more or less complicated patterns and both the amplitude and phase delay (the phase angle of signal reception) can increase or decrease. If the disturbance occurs during daytime, its cause is most likely the incidence of solar X-ray radiation in the lower ionosphere. The incidence of solar X-ray radiation in the upper VLF waveguide boundary can cause a) the "sharpening" and the descending of the lower edge of the ionosphere (the upper boundary of the VLF waveguide) due to electron density increase, or b) increasing of the total electron content in the whole D-region without the "sharpening" of the lower edge of the ionosphere.

In case a) the so called "mirror" type of VLF signal reflection occurs, because of the reflecting surface, in terms of electrical conductivity, behaves as metal. Energy dissipation of incidence VLF wave is negligible, even less than that in unperturbed ionospheric conditions. Such disturbances in the waveguide cause an increase of registered VLF signal amplitude. The reflected VLF signal amplitude changing follows the X-ray radiation intensity changes during the flare event: the amplitude relatively rapidly increases until it reaches its maximal value and then gradually decreases until it reaches the value that corresponds to the unperturbed value of the amplitude before



the flare event impact. In case b) VLF signal penetrates into the D-region up to the altitude where VLF signal frequency equalizes to plasma frequency which is the site of VLF signal reflection. Along the part of the path which is inside D-region, refraction coefficient of VLF signal varies from one point to another with constant energy dissipation, depending on VLF signal frequency (deviant absorption, (Budden, 1988)). Reflected VLF signal leaves lower ionospheric boundary with energy lower than that of incident signal. In this case, rapid electron density increase in the lower ionosphere due to the incidence of X-ray radiation during solar flare is followed by rapid VLF signal amplitude decrease until the amplitude reaches its minimal value and then VLF propagation parameters go back to the values that correspond to unperturbed regular conditions in the lower ionosphere.

As a result of the phase trajectory shortening over the GCP due to VLF signal reflection height lowering during the flare event impact, the location of the main modal minimum (and of all others, as well) on the signal trace is moved toward the transmitter site. There are fewer wavelengths on the shortened trajectory, which correspond to a smaller delay in phase, therefore a higher phase angle. On the other hand, VLF signal penetrations into the D-region cause a phase trajectory elongation by each VLF signal reflection from the ionosphere, which correspond to a greater delay in the phase, therefore a smaller phase angle.

The value of the registered VLF signal amplitude is also affected by the interference modes layout along the GCP and thus by vicinity of the modal minima and maxima to the receiver site as well. The increase in the amplitude, which is characteristic for the case a), is going to be more pronounced if the receiver is placed in the vicinity of a modal maximum than if it is placed in the vicinity of a modal minimum. Moreover, if the receiver is placed in the vicinity of a modal maximum, the decrease in amplitude, which is characteristic for the case b), is going to be less pronounced than if the receiver is placed in the vicinity of a modal minimum. The sign of the phase delay change (phase trajectory shortening or elongating) depends on the interference modes layout along the GCP, too, but also depends on the length of the VLF signal path.

The amount of amplitude and phase delay changes during flare state depends on the redistribution of the local minima and maxima locations along the signal trace compared to the regular unperturbed state in the waveguide. The distance between the transmitter and the receiver along the GCP (the number of signal reflections in the waveguide) and the incidence angle at the

lower D-region boundary affect the behavior of the signal, especially in the perturbed ionospheric conditions. The phase trajectory modification is the result of both effects. In most cases, GQD signal penetrates into the area of an increased electron density above the lower D-region boundary, where the deviant energy absorption takes place, which manifests at the receiver site as the GQD signal amplitude decreases, compared to the preflare and postflare states, as in case of C9.7 and C4.8 flare events. GQD signal reflection of the "mirror" type occurs only in the case of higher class X-ray solar flare events and it is only related to the moments of maximal X-ray irradiance, such as in cases of M2.5 and C9.6 flare events.

Although the effects on VLF signal amplitude and phase delay which are induced by X-ray solar flare events can always be clearly noticed and recognized, the flare events with the same characteristics (class, duration, zenith angle of incidence radiation) can cause different types of amplitude and phase delay perturbations depending on which VLF signal trace it is monitored. For example, all four flare events which have been analyzed in this paper on GQD signal, in case of NAA/24.0 kHz signal (the GCP distance 6540 km) are characterized with "mirror" type of VLF signal reflection at the Belgrade receiver site (Kolarski et al., 2011). "Mirror" type of signal reflection is characteristic for NAA signal received at the Belgrade receiver site regardless of the flare event strength (Kolarski et al., 2011).

### 3. Conclusions

The aim of this paper was an extended comparative qualitative analysis regarding the behavior of D-region electron population during the four analyzed X-ray solar flare events that impacted the lower ionosphere VLF propagation on a GQD signal trace. We analyzed patterns that occur on a GQD signal during these solar X-ray flares depending on the X-ray solar flare event's strength and the changes in amplitude and phase delay modal minima and maxima movements along the GCP caused by these X-ray solar flare events. We have also analyzed the electron density change responses during the whole time period that X-ray solar flares impacted transmissions on GQD signal and electron density height profiles throughout D-region, in the altitude domain around the signal reflection heights where Wait theory can be applied in a reliable manner. The application of Wait theory to the boundaries of ionospheric region considered is somewhat unrealistic, thus the results concerning ionospheric D-region bottom and top should be taken with

caution and were analyzed only in the sense to provide general insight into electron population behavior, i.e. trend of changes. This is significantly more important during the X-ray solar flare event's impact.

Each analyzed flare event impact on GQD signal amplitude and phase delay is specific. In general, the amplitude decrease, due to deviant energy absorption, followed by the phase delay increase, occurs as the result of VLF signal reflection height lowering. Such perturbations can be seen in cases of solar flare events, which occurred on 07 April, 2006 and on 06 December, 2006. Different type of perturbations took place at flare peaks occurred on 06 July, 2006 and on 07 September, 2005. In these cases, after short-lasting decrease, the amplitude increases until it reaches its maximal value above the regular ionospheric conditions level, while simultaneously phase delay decreases until it reaches its minimal value. It is clear that amplitude increases due to the "mirror" type of VLF signal reflection, as simultaneously reflecting height lowers and phase trajectory shortens. But, instead of the decrease, increase of the delay in the phase occurred, so the GQD signal phase descends. The amount of these changes depends on the solar flare event class, and also on the modal extremes distribution along the GCP, therefore, on electron density height profile at a certain moment and at a certain location in the waveguide.

#### **4. Acknowledgments**

The authors wish to acknowledge insightful comments and suggestions and valuable discussions on this topic with A. Nina and V. Čadež in preparing this manuscript. The authors appreciate comments expressed by all referees, which have led to significant improvements in the contents of this paper. The thanks are due to Ministry of Science and Technological Development of Serbia, project III 44002.

#### **5. References**

##### **References**

- Appleton, E. V., A note on sluggishness of ionosphere, *J. Atmos. Sol.-Terr. Phy.*, 3, pp. 282-284, 1953.
- Balan, N., Alleyne, H., Walker, S., Reme, H., McCrea, I., Aylward, A., Magnetosphere-ionosphere coupling during the CME events of 07-12 November 2004, *J. Atmos. Sol.-Terr. Phy.*, 70, 2101-2111, 2008.

- Basak, T., Chakrabarti, S. K., Effective recombination coefficient and solar zenith angle effects on low-latitude D-region ionosphere evaluated from VLF signal amplitude and its time delay during X-ray solar flares, *Astrophys. Space. Sci.* 348 (2), 315-326, 2013.
- Belenkiy, M. I., Orlov, A. B., Petrova, G. A., Uvarov, A. N., Modeling of the electron density profile of the lower ionosphere (45-75 km) for sudden ionospheric disturbance conditions based on the data on sudden phase anomalies of VLF signals, *Int. J. Geomagn. Aeron.*, 6, GI3007, 2006.
- Budden, K. G., *The propagation of radio waves*, (Cambridge University Press, Great Britain, 1988).
- Chakrabarti, S. K., Mandal, S. K., Sasmal, S., Bhowmick, D., Choudhury, A. K., Patra, N. N., First VLF detections of ionospheric disturbances due to Soft Gamma Ray Repeater SGR J1550-5418 and Gamma Ray Burst GRB 090424, *Indian Journal of Physics*, 84, 1461-1466, 2010.
- Chakrabarti, S. K., Mondal, S. K., Sasmal, S., Pal, S., Basak, T., Chakrabarti, S., Bhowmick, D., Ray, S., Maji, S. K., Nandy, A., Yadav, V. K., Kotoch, T. B., Khadka, B., Giri, K., Garain, S. K., Choudhury, A. K., Partra, N. N., Iqbal, N., VLF signals in summer and winter in Indian sub-continent using multi-station campaigns, *Indian J. Phys.*, 86 (5), 323-334, 2012.
- Chakrabarti, S. K., Pal, S., Sasmal, S., Mondal, S. K., Ray, S., Basak, T., Maji, S. K., Khadka, B., Bhowmick, D., Chowdhury, A. K., VLF campaign during the total eclipse of July 22nd, 2009: Observational results and interpretations, *J. Atmos. Sol.-Terr. Phys.*, 86, 65-70, 2012.
- Ferguson, J. A., *Computer Program for Assessment of Long-Wavelength Radio Communications, Version 2.0.*, (Space and Naval Warfare Systems Center, San Diego, CA, 1998).
- Grubor, D. P., Šulić, D. M., Žigman, V., Classification of X-ray solar flares regarding their effects on the lower ionosphere electron density profile, *Ann. Geophys.*, 26, 1731-1740, 2008.
- Inan, U. S., Lehtinen, N. G., Moore, R. C., Hurley, K., Boggs, S., Smith, D. M., Fishman, G. J., Massive disturbance of the daytime lower ionosphere

- by the giant  $\gamma$ -ray flare from magnetar SGR 1806-20, *Geophys. Res. Lett.*, 34, 8103-8108, 2007.
- Kolarski, A., Grubor, D., Šulić, D., Diagnostics of the solar X-flares impact on the lower ionosphere through seasons based on VLF-NAA signal recordings, *Baltic Astronomy*, 20, 591-595, 2011.
- McKinnell, L. A., Friedrich, M., A neural network-based ionospheric model for the auroral zone, *J. Atmos. Sol.-Terr. Phy.*, 69, 1459-1470, 2007.
- McRae, W. M., Thomson, N. R., VLF phase and amplitude: daytime ionospheric parameters, *J. Atmos. Sol.-Terr. Phy.*, 62, pp. 609-618, 2000.
- McRae, W. M., Thomson, N. R., Solar flare induced ionospheric D-region enhancements from VLF amplitude observations, *J. Atmos. Sol.-Terr. Phy.*, 66, pp. 77-87, 2004.
- Mitra, A. P., *Ionospheric Effects of Solar Flares*, VOL. 46 (Astrophysics and space science library, D. Reidel publishing Company, Boston, 1974).
- Nina, A., Čadež, V., Srećković, V. A., Šulić, D., The Influence of Solar Spectral Lines on Electron Concentration in Terrestrial Ionosphere, *Baltic Astronomy*, 20, 609-612, 2011.
- Nina, A., Čadež, V., Srećković, V. A., Šulić, D., Altitude distribution of electron concentration in ionospheric D-region in presence of time-varying solar radiation flux, *Nucl. Instrum. Meth. B*, 279, 110-113, 2012.
- Nina, A., Čadež, V., Srećković, V. A., Žigman V., Effective electron recombination coefficient in ionospheric D-region during the relaxation regime after solar flare from February 18, 2011, *Nucl. Instrum. Meth. B*, 279, 106-109, 2012.
- Nina, A., Čadež, V., Detection of acoustic-gravity waves in lower ionosphere by VLF radio waves, *Geophys. Res. Lett.*, 40 (18), 4803-4807, 2013.
- Nina, A., Čadež, V., Electron production by solar Ly- $\alpha$  line radiation in the ionospheric D-region, *Adv. Space Res.*, 2014, <http://dx.doi.org/10.1016/j.asr.2013.12.042>.

- Pal, S., Chakrabarti, S. K., Theoretical models for computing VLF wave amplitude and phase and their applications, AIP Conf. Proc., 1286, 42-60, 2010.
- Palit, S., Basak, T., Mondal, S. K., Pal, S., Chakrabarti, S. K., Modeling of very low frequency (VLF) radio wave signal profile due to solar flares using the GEANT4 Monte carlo simulation coupled with ionospheric chemistry, Atmos. Chem. Phys., 13, 9159-9168, 2013.
- Ratcliffe, J. A., *An introduction to the ionosphere and magnetosphere*, (Cambridge University Press, Great Britain, 1972).
- Tanaka, Y. T., VLF observations of magnetar flares, AIP Conf. Proc., 1286, 331-338, 2010.
- Thomson, N. R., Experimental daytime VLF ionospheric parameters, J. Atmos. Sol.-Terr. Phys., 55 (2), pp. 173-184, 1993.
- Thomson, N. R., Rodger, C. J., Clilverd, M. A., Large solar flares and their ionospheric D region enhancements, J. Geophys. Res., VOL. 110, A06306, 2005.
- Thomson, N. R., Rodger, C. J., Clilverd, M. A., Daytime D region parameters from long-path VLF phase and amplitude, J. Geophys. Res. 116, 11305-11310, 2011.
- Wait, J. R., Spies, K. P., *Characteristics of the Earth-ionosphere waveguide for VLF radio waves*, (NBS Technical Note 300, 1964).
- Whitten, R. C., Poppoff, I. G., *Physics of the Lower Ionosphere*, (Englewood Cliffs, N. J. Prentice-Hall, 1965).
- Žigman, V., Grubor, D., Šulić, D., D-region electron density evaluated from VLF amplitude time delay during X-ray solar flares, J. Atmos. Sol.-Terr. Phys., 69, pp. 775-792, 2007.

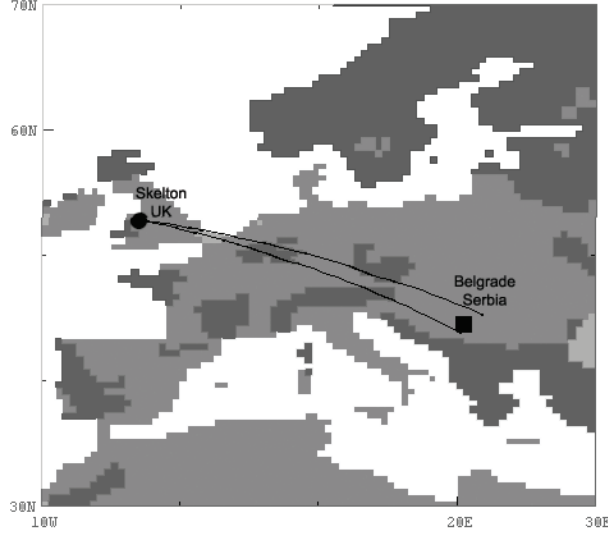


Figure 1: Possible paths for GQD/22.1 kHz VLF signals emitted from Skelton (UK) toward Belgrade (Serbia).

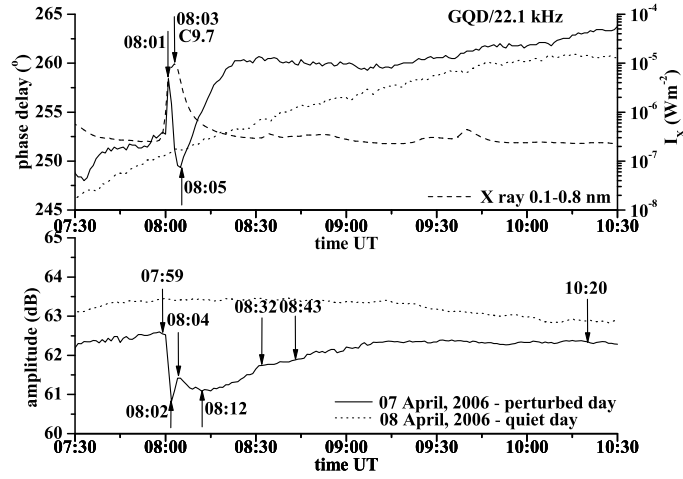


Figure 2: GQD signal perturbation during C9.7 class X-ray solar flare event.



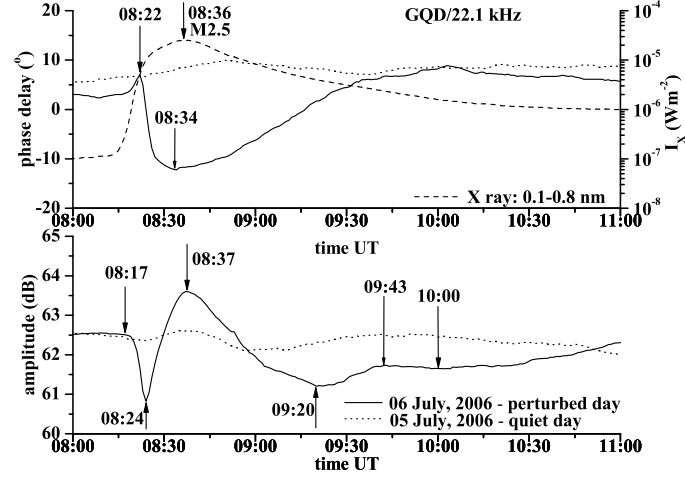


Figure 3: GQD signal perturbation during M2.5 class X-ray solar flare event.

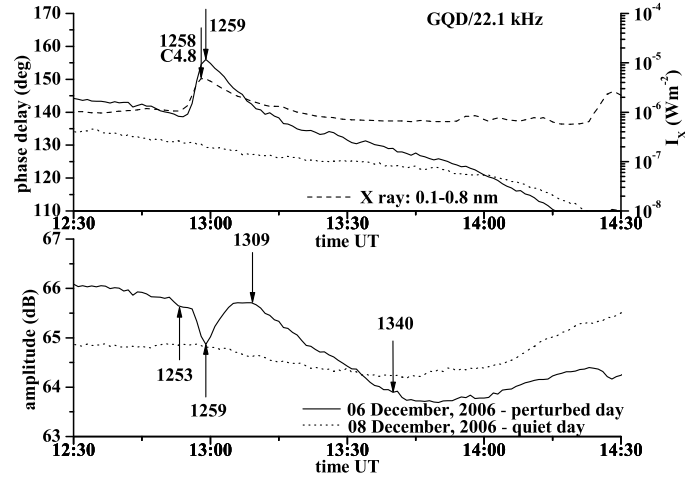


Figure 4: GQD signal perturbation during C4.8 class X-ray solar flare event.

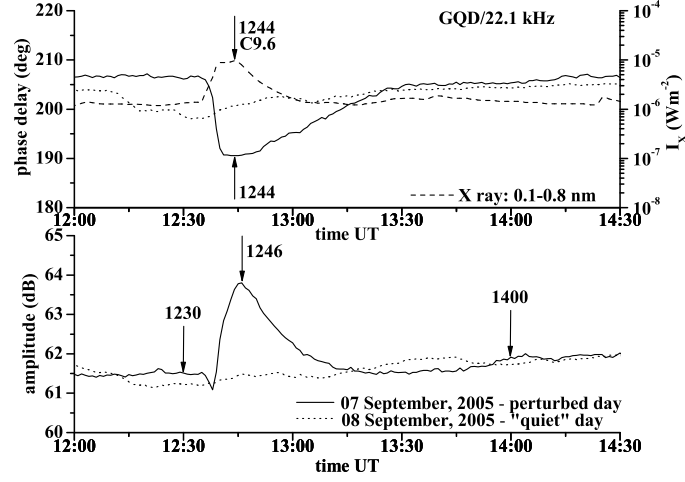


Figure 5: GQD signal perturbation during C9.6 class X-ray solar flare event.

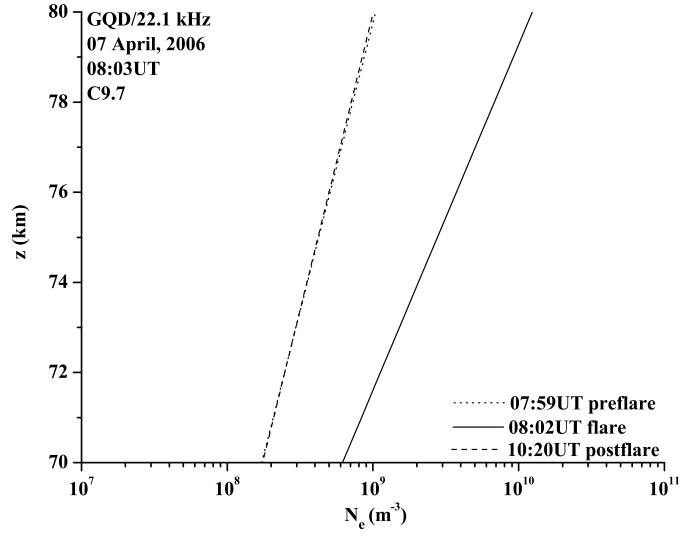


Figure 6: Electron density height profiles during C9.7 class X-ray solar flare event.

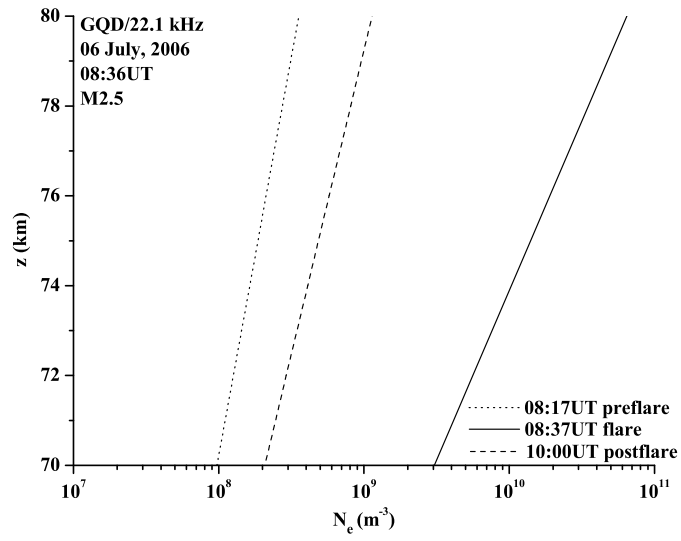


Figure 7: Electron density height profiles during M2.5 class X-ray solar flare event.

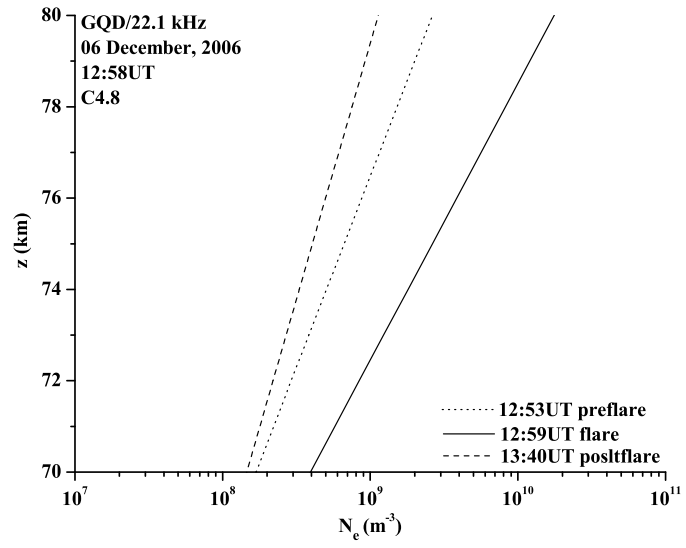


Figure 8: Electron density height profiles during C4.8 class X-ray solar flare event.

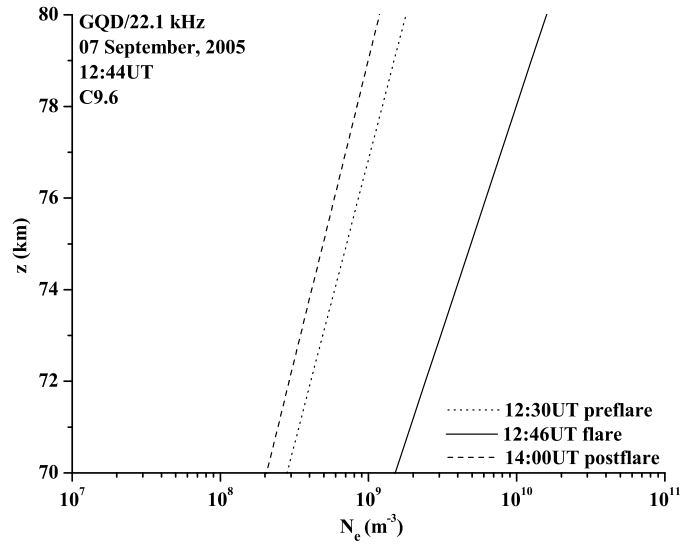


Figure 9: Electron density height profiles during C9.6 class X-ray solar flare event.

Table 1: The flare events below are observed on the analyzed GQD/22.1 kHz signal traces

date	time (UT)	class	$I_{xmax}$ (Wm <sup>-2</sup> )	quiet day
07 Apr. 2006	08:03	C9.7	$9.74 \cdot 10^{-6}$	08 Apr. 2006
06 July 2006	08:36	M2.5	$2.51 \cdot 10^{-5}$	05 July 2006
06 Dec. 2006	12:58	C4.8	$4.82 \cdot 10^{-6}$	08 Dec. 2006
07 Sep. 2005	12:24	C9.6	$9.62 \cdot 10^{-6}$	08 Sep. 2005

Table 2: Parameters characterizing GQD/22.1 kHz signal propagation conditions for the X-ray solar flare events considered

flare event	time (UT)	state	$\Delta A$ (dB)	$\Delta P$ (°)	$N_e(74 \text{ km})$ ( $\text{m}^{-3}$ )
07 Apr. 2006 08:03UT C9.7	07:59	preflare	-0.89	2.52	$3.54 \cdot 10^8$
	08:01	$P_{max}$	-1.72	7.68	$8.61 \cdot 10^8$
	08:02	flare $A_{min1}$	-2.62	4.93	$2.05 \cdot 10^9$
	08:04	$A_{max1}$	-1.98	-1.69	$5.90 \cdot 10^8$
	08:05	$P_{min}$	-1.99	-1.78	$5.90 \cdot 10^8$
	08:12	$A_{min2}$	-2.34	3.09	$1.04 \cdot 10^9$
	08:32	$A_{max2}$	-1.71	6.28	$8.61 \cdot 10^8$
	08:43	$A_{min3}$	-1.55	4.48	$6.56 \cdot 10^8$
	10:20	postflare	-0.53	2.31	$3.52 \cdot 10^8$
06 July 2006 08:36UT M2.5	08:17	preflare	0.04	-3.44	$1.63 \cdot 10^8$
	08:22	$P_{max}$	-0.72	0.11	$4.10 \cdot 10^8$
	08:24	$A_{min1}$	-1.54	-6.46	$1.56 \cdot 10^9$
	08:34	$P_{min}$	0.76	-20.34	$1.08 \cdot 10^{10}$
	08:37	flare $A_{max1}$	1.0	-20.25	$1.03 \cdot 10^{10}$
	09:20	$A_{min2}$	-1.11	-6.54	$8.25 \cdot 10^8$
	09:43	$A_{max2}$	-0.79	-0.99	$4.10 \cdot 10^8$
	10:00	postflare	-0.79	-0.44	$4.10 \cdot 10^8$
06 Dec. 2006 12:58UT C4.8	12:53	preflare	0.8	7.44	$5.06 \cdot 10^8$
	12:59	flare $A_{min}, P_{max}$	0.06	26.71	$1.80 \cdot 10^9$
	13:09	$A_{max}$	1.09	15.41	$1.04 \cdot 10^9$
	13:40	postflare	-0.33	5.51	$3.31 \cdot 10^8$
07 Sep. 2005 12:44UT C9.6	12:30	preflare	0.29	2.09	$5.90 \cdot 10^8$
	12:46	flare $A_{max}, P_{min}$	2.32	-13.33	$3.88 \cdot 10^9$
	14:00	postflare	0.19	1.36	$4.14 \cdot 10^8$



Table 3: Simulation results of GQD signal propagation along the GCP for the X-ray solar flare events considered

flare event class	C9.7	M2.5	C9.6	C4.8
$D_{preflare}$ (km)	740	760	700	960
$D_{flare}$ (km)	700	600	600	940
$D_{postflare}$ (km)	740	720	720	960
main mod. min. in flare state	$\uparrow$	$\uparrow$	$\uparrow$	no change
$r$	$\cong 1$	$< 1$	$\cong 1$	$\cong 1^*$
$\Delta D$ (km)	$\cong 0$	$< 0$	$> 0$	$\cong 0^*$
$\Delta D_f$ (km)	40	160	100	20*
additional mod. min.	no**	yes	yes	no
preflare ionospheric conditions	regular	regular	perturbed	perturbed